Structural and optical properties of rare-earths doped barium bismuth borate glasses

Silvia Barbi[a,*], Consuelo Mugoni[b], Monia Montorsi[c], Mario Affatigato[d], Corrado Gatto[e], Cristina Siligardi[b]

[a] Interdepartmental Center for Applied Research and Services in Advanced Mechanics and Motoring, 41125 Modena, Italy
[b] Department of Engineering "E. Ferrari", University of Modena and Reggio Emilia, 41125 Modena, Italy
[c] Department of Science and Methods for Engineering, University of Modena and Reggio Emilia, 42122 Reggio Emilia, Italy
[d] Physics Department, Coe College, Cedar Rapids, IA 52402, United States
[e] Istituto Nazionale Di Fisica Nucleare, Sezione di Napoli, Italy

ARTICLE INFO

Keywords:
Structure
Glasses
Borate
Rare-earths

ABSTRACT

Recently, great importance has been devoted to different glass systems doped with rare-earth ions because of their peculiar properties, in particular in the field of high-energy physics for particle energy measurement. The purpose of the present study was to investigate the optical and physical properties of Dy^{3+}, Er^{3+}, Nd^{3+} doped glasses belonging to the $20BaO\text{-}20Bi_2O_3\text{-}60B_2O_3$ system in which several rare-earths oxide concentrations were added to encounter the requirements for particle energy measurement. High density, low refractive index, high emission intensity (or high scintillation yield) are required for this purpose. Moreover, molar volume, glass transition and melting temperatures, X-ray diffraction and Raman spectra were measured and discussed in order to characterize the glass state. All the properties measured have shown a non-linear trend moving from 1 mol% to 10 mol% of rare-earths content. At the same time comparison between the trend derived by samples with same stoichiometry but containing different rare earths highlight different behaviors. In particular the highest density has been reached with the glass where Dy_2O_3 is at 2,5 mol%.

1. Introduction

The more recent discoveries in particle physic have been reached during development of innovative materials. Glasses suitable for hadronic calorimeter can be absolutely part of this group of materials because, thanks to its optical property, they can substitute very high priced single crystal detectors, opening to further possibilities in this research field. Historically, visual scintillation was employed through materials such as $CaWO_4$ [1,2] and ZnS [3] during the Rutherford's experiment. Taking in account the new generation of high energy physics (HEP) experiments the development of suitable scintillators such as bismuth germanate (BGO) [4], cesium iodide (CsI) [5–8], barium fluoride (BaF_2) [9,10], cerium fluoride (CeF_3) [11,12] and lead tungstate, $PbWO_4$, (PWO) [13,14] played a key role. Nowadays, modern detectors require very tight specifications that need multi-disciplinary efforts to develop suitable scintillators at an industrial scale. The improvements about scintillating material in HEP could be one of the key point to develop faster and more efficient devices for other application such as industrial and medical imaging devices. Three key points are fundamental to select luminescent material suitable for HEP [15,16]: density, scintillation properties, cost and environmental sustainability. The density of such material has to be higher than > 5 g/cm^3 to favor high compactness of the calorimeter which is essential to reduce the detector volume and high density results in an increased X-ray absorption cross-section and the signal-to-noise ratio [17–18]. A compact material will reduce the lateral spread of the shower in a high-magnetic field. Moreover, the stopping power of the materials, on the particles to be detected, is related to the compactness of the crystal lattice, keeping the atomic number (Z) of the component not too large, in order to reduce the lateral shower size. In fact, usually the Moliere Radius (R_m) is taken into account in the design of materials for calorimeters, because a small R_m means lower contamination of the energy measurement by other particles, which help for position reconstruction. R_m is defined experimentally by the equation $R_m \approx X_0 (Z + 1.2) / 37.74$ where X_0 is the radiation length. In high density material $\times_0$ is usually small and also Z must be not too large, to obtain a small R_m.

About the scintillation properties and radiation hardness, in order to

* Corresponding author.
E-mail address: silvia.barbi@unimore.it (S. Barbi).

obtain strong data from the particle detector, the emission light yield and the energy resolution must be as much high as possible. The emission light yield is also dependent by the geometry of the calorimeter and generally a light emission in the UV–VIS area will reduce the problems of light collection, for this reason the optical transmittance of the material in the UV–VIS region should be very high. The energy resolution of the calorimeter is affected by any source of non-uniformity of the material. For this reason, intrinsic scintillators materials should be preferred as it is easier to control the light yield uniformity in long geometry, and a controlled distribution of the doping scintillating compound could help to correct non-uniformity in the light collection in a pointing geometry. The light collection in a pointing geometry will introduce non-uniformity due to the focusing effect, which depends on the refractive index of the material. Fluoride crystals and glasses, with refractive index around 1.5, will limit this effect to a much smaller value (and therefore make it much easier to correct) than for the BGO (refractive index 2.15) or PWO (refractive index 2.3) [13,14].

Although hadronic calorimeters cover a market niche, their costs and environmental sustainability become fundamental due to the large volume (several cubic meters) used for such detectors. The main costs associate to the detector development derives from the raw materials and its manipulation to obtain the suitable final material, as well as from the cost of disposal or recycle. For example, notwithstanding the high efficiency of lutetium crystal for HEP, its application was discarded due to the high cost of the raw material. On the contrary, based on economic perspective, cerium and lead represent a valid choice due to their easy availability on the market at low prices. Moreover, considering the costs of the energy, crystals that can be grown with cheap methods and low-cost crucibles are favorable than the others. In order to limit also the processability costs crystals or glasses with low melting point but good mechanical properties, such as some lead compound (PbF_2 and $PbWO_4$), was used [13,14]. Recently environmental sustainability studies have been taken in account into the materials criteria selection for HEP and lead-free samples will be favored.

Considering glasses materials one of the main challenging point is about density that have to be higher than 5 g/cm^3 in hadronic calorimeter detectors to detect the particles. Unfortunately, the typical density of glass, such as silicate glass, is around 2–3 g/cm^3. Moreover, the scintillating properties of these materials must be enhanced through the use of dopants homogeneously distributed avoiding presence of aggregates, impurities or crystalline phases. For this reason, also the structural properties must be properly considered. Starting from high density and enhanced scintillating properties that are required for hadronic calorimeter respectively, heavy metals and rare earths (RE) have been mixed in order to obtain glasses. Specifically, Dy_2O_3, Nd_2O_3 and Er_2O_3 have been chosen as dopants according to the wide literatures in which these oxides have been commonly used in optical application [19–31]. Therefore, the purpose of the present study was to investigate how different rare earths such as Dy^{3+}, Er^{3+}, Nd^{3+} affect the glass density properties of a barium bismuth borate base glass encountering one of the main requirement for the investigated application. Furthermore the luminescent properties were evaluated as a function of rare-earths oxide concentrations. Beyond the very specific behavior of the rare earths considered, also the influence of the base glass must be taken in account to avoid potential undesired effects such as quenching. Compositional (three different dopants) and concentration effect of RE were systematically investigated starting from a basic glass: 20BaO-20Bi_2O_3-60B_2O_3. In particular density, refractive index (RI), optical transmittance and emission intensity have been investigated and discussed considering the requirements needed for HEP and their possible employment. Moreover, molar volume, glass transition and melting temperatures, X-ray diffraction, and Raman spectra have been measured and discussed in order to correlate the glass state with the final optical properties.

Table 1
List of the investigated glass compositions (mol%).

Series with Dy_2O_3 as rare earth (A)				
Sample	BaO	Bi_2O_3	B_2O_3	Dy_2O_3
A1	20	19	60	1
A2	20	17.5	60	2.5
A5	20	15	60	5
A7	20	12.5	60	7.5
A10	20	10	60	10
Series with Er_2O_3 as rare earth (B)				
Sample	BaO	Bi_2O_3	B_2O_3	Er_2O_3
B1	20	19	60	1
B2	20	17.5	60	2.5
B5	20	15	60	5
B7	20	12.5	60	7.5
B10	20	10	60	10
Series with Nd_2O_3 as rare earth (C)				
Sample	BaO	Bi_2O_3	B_2O_3	Nd_2O_3
C1	20	19	60	1
C2	20	17.5	60	2.5
C5	20	15	60	5
C7	20	12.5	60	7.5
C10	20	10	60	10
Glass without rare earths (U)				
Sample	BaO	Bi_2O_3	B_2O_3	RE
U	20	20	60	0

2. Materials and methods

2.1. Glasses formulation

In this work several glasses have been melted starting from reagent grade compounds from Sigma-Aldrich. In particular the following raw materials have been employed: BaO (Sigma-Aldrich, 99.99%), Bi_2O_3 (Sigma-Aldrich, 99.99%), B_2O_3 (Sigma-Aldrich, 99.97%), Dy_2O_3 (Sigma-Aldrich, 99.9%), Nd_2O_3 (Sigma-Aldrich, 99.9%), Er_2O_3 (Sigma-Aldrich, 99.9%). The starting point from which the glasses formulation have been chosen must be found in bibliographic research [32–37] and consist of the following glasses formulation 20BaO-(20-x) Bi_2O_3-60B_2O_3-xRE_2O_3. In Table 1 the list of all the glasses melted and characterized.

Glass samples have been prepared by conventional melt-quenching technique. The components have been mixed together for 15 min in an alumina jar, put in a platinum crucible and melted from room to the melting temperature (1000 °C to 1250 °C depending on the composition) for 90 min, with a heating cycle of 10 °C per minute. The crucible has been shaken once after the first 90 min of the melting for the homogeneous mixing of all the constituents. The melting process was conducted in a Pt crucible instead of alumina to avoid any possible reaction with the borate melts that could potentially lead to drastic decrease of the final density by destruction of tetrahedral boron species Subsequently, the melt was poured through plate quenching technique and the obtained samples were annealed at 10 °C below their glass transition temperature (T_g) in order to relieve the thermal stress and to reduce the number of the defects thus, improving the transmittance of the final glassy materials. In this study, the melting temperature has been evaluated experimentally, observing the behavior of each glass at high temperature to keep the melted glass as much homogeneous as possible. In fact, as also already reported in literature, glasses containing bismuth oxide forms metallic bismuth when the melting

temperature reaches 1300 °C [38]. Other studies reported also that Bismuth has several kinds of valence states simultaneously existing in glasses and this could affect the luminescence properties. The various emission centers in bismuth glasses depend by the various ionic species (e.g., Bi^{5+}, Bi^{3+}, Bi^{2+} and Bi^{+}) [39–45]. The various valence states of bismuth take place by the auto-thermo reduction of Bi^{3+} ions that proceeds towards metallic Bismuth reversibly during melting process, through the following intermediate valence states:

$Bi^{3+} \leftrightarrow Bi^{2+} \leftrightarrow Bi^{+} \leftrightarrow$ Bi metallic

Up to now, it is not clear which valence of bismuth ion contributes to the various emissions. The blue to green region emission has been reported by Bi^{3+} ions, whereas the red emission is due to Bi^{2+} ionic species. Apart from this case the absolutely complete melting of all the components is necessary and for this reason the melting temperature change slightly from glass to glass depending on the amount of rare earth into the glass formulation. The highest melting temperatures have been reached for the glasses containing the highest amount of rare earths: A10, B10, C10. All the glasses were poured through plate quenching technique in order to obtain slight samples (thickness = 1 mm) and annealed around the glass transition temperature to remove thermal stress, employing steel plates pre-heated to 400 °C and annealed in furnace for 2 h. From experimental observation, an annealing temperature of 400 °C has been evaluated as suitable for all the samples investigated in this study. The thickness of the samples, equal to 1 mm, has been chosen as the lower possible in order to enhance the optical transmission and taking in account the typical values of thickness employed in scintillating materials for high energy physics.

2.2. Glasses characterization

All the glasses listed in paragraph 2.1 have been characterized by means of density, molar volume, thermal behavior, Raman spectroscopy, X-ray diffraction, RI, emission intensity, UV–VIS transmittance and scintillating yield, in order to correlate the physical and optical properties with the glass structure and to identify the most suitable formulation for HEP experiments.

In details, the density has been measured through helium pycnometer (Quanta Chrome - Micropycnometer). In this way at least 1 cm^3 of glass has been employed to perform the measure, and the results obtained for each glass are achieved through 15 measurements of the same specimens. The density associated to each sample is a result of average value calculation and the relative error is the standard deviation calculated on 15 measurements. From the average values of density measurements also the molar volume (V_m) has been calculated for each glass following the formula:

$$V_m = \frac{\sum_i^n x_i m_i}{\rho} \qquad \left[\frac{cm^3}{mol}\right]$$

where x is the molar fraction and m is the weight of each component (i) of the formulation of the glass and ρ is the measured density. The same error calculated for the average value of density has been associated to molar volume. The thermal behavior of each glass was measured using DSC analysis (Netzsch, DSC 404) performed in air at the heating rate of 10 °C/min on sample ground to an average particle size of < 30 μm. The DSC measurements have been carried out on ca. 30 mg of sample in a Pt crucible. The glass transition temperature (Tg) has been calculated as the crosspoint between the tangent on the initial straight line before baseline shifting and the tangent on the slope. The evaluated error on this measurement is associated with the sensitivity of the instrument (10 °C).

Raman scattering spectra of the glasses were measured at room temperature with a laser Raman spectroscopy (JASCO Co., NRS-3100) with solid state laser (520) nm wavelength. All the Raman spectra are normalized to allow the spectra comparison.

The structural properties have been investigating also through X-ray diffraction (XRD, Bruker) at room temperature by packing the finely ground samples into an aluminum sample holder at room temperature from and scanning from 2θ = 10 to 75° with a step size of 0.01°2θ.

The optical properties that have been measured are Refractive Index and Emission (Luminescence) Intensity. RI has been measured through Abbe refractometer (ATAGO, NAR 1T-Solid) on the glass as it quenched. The range of values detectable is 1.300 to 1.700. The instrument sensitivity (0.001) has been taken as error on the measured value. A JASCO FP6500 Spectrofluorometer has been used to measure the fluorescence spectra. The spectrometer has been equipped with Xe lamp and photomultiplier tube as detector. The measured wavelength range has been 220–750 nm with a resolution of 1 nm. The error on the measured intensity can be considered as 1%. Only for selected glasses a further optical characterization has been performed, UV–VIS transmittance. The optical transmittance spectra in the range 400–700 nm have been obtained using a UV–VIS spectrometer Ocean Optics, USB4000-XR1 / DH-2000-BAL employing 4 mm thickness of sample. All the characterizations described up to now have been performed at room temperature. The optical properties such as optical transmittance and photoluminescence have been evaluated only in the UV–VIS range because this is the range in which we are interested, considering the purpose of the present paper. On selected samples the scintillation light yield measurement has been performed using 1350 V from a ^{207}Bi source through a photomultiplier as photodetector (Hamamatsu 669). pT (*p*-terphenyl) and DMPOPOP (dymethil-POPOP) has been used as standard blue for reference [46].

3. Results

3.1. Structural properties: X-ray diffraction (XRD) and Raman spectroscopy

In Fig. 1 the XRD pattern of the sample U is shown. From Figs. 2 to 4 the XRD glasses of the doped glasses are shown. The XRD patterns are sorted considering the rare earth employed as dopant.

The XRD patterns show a totally glassy state for each sample with the exception of C7 and C10 (Nd_2O_3 content higher than 7.5 mol%). Furthermore from Fig. 1 to Fig. 4 a glassy broad band around 28°2θ can be observed. A strong decreasing of intensity of that glassy band can be observed in all the three series of samples, if the dopant is the amount of 5%. The Raman spectra of all the glasses are reported in Figs. 5, 6, 7 and 8: compositional effect (different dopant) and concentration trend (same dopant) have been analyzed in comparison to the sample U in which no dopant is present in glass composition.

The Raman spectrum of the sample U, reported in fig. 5, suggests that this family of glasses is characterized by two main glassy band: the first at intermediate regions of frequencies (150–700 cm^{-1}) and a second at higher frequencies (1100 to 1800 cm^{-1}). It is worth noting

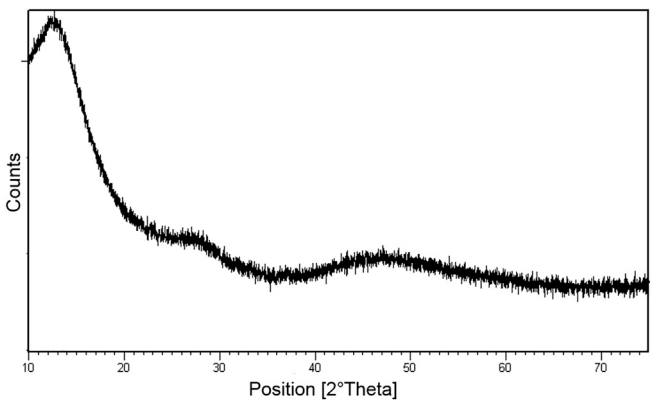

Fig. 1. XRD pattern of the glass U.

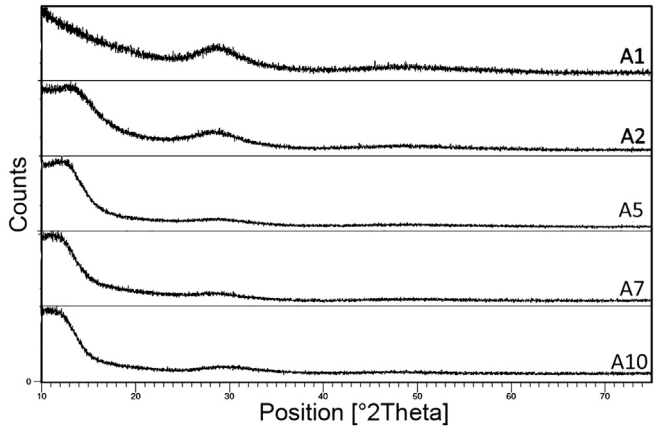

Fig. 2. XRD patterns of the glasses of the series A (x from 1 to 10 mol%).

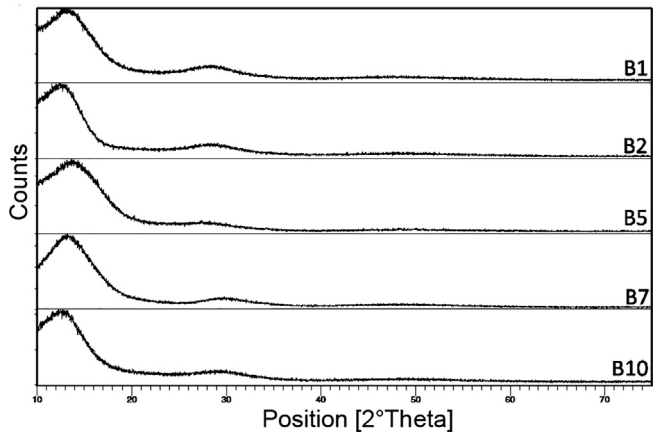

Fig. 3. XRD patterns of the glasses of the series B (x from 1 to 10 mol%).

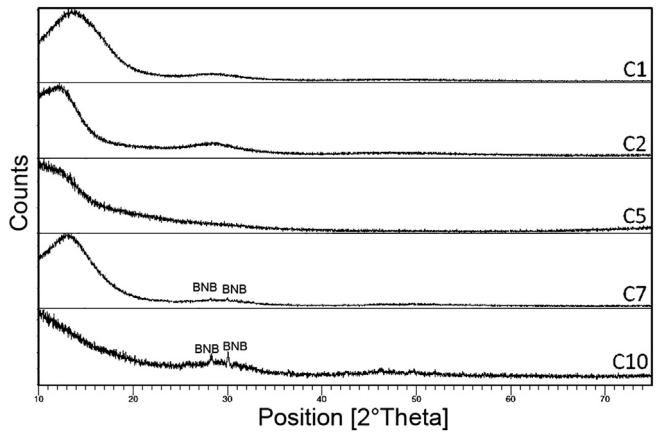

Fig. 4. XRD patterns of the glasses of the series C (x from 1 to 10 mol%). The founded crystalline phase is Barium Neodymium Borate (ICCD: 01–084-1358) labelled as BNB.

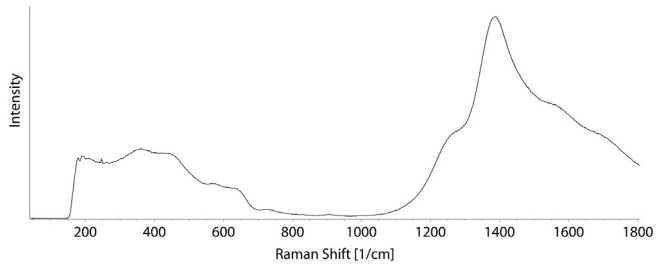

Fig. 5. Raman spectrum of the glass U.

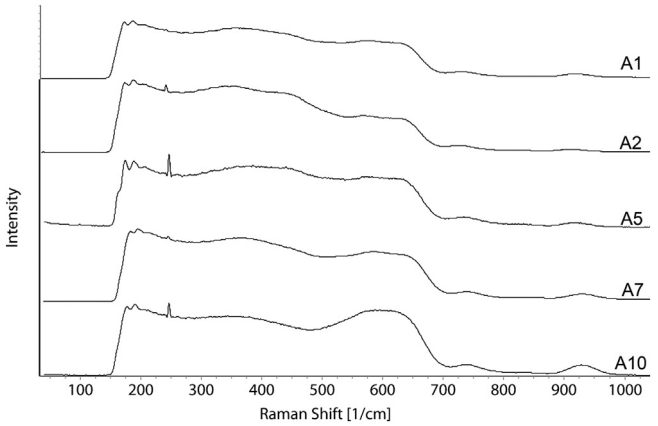

Fig. 6. Raman spectra of the series A (x from 1 to 10 mol%).

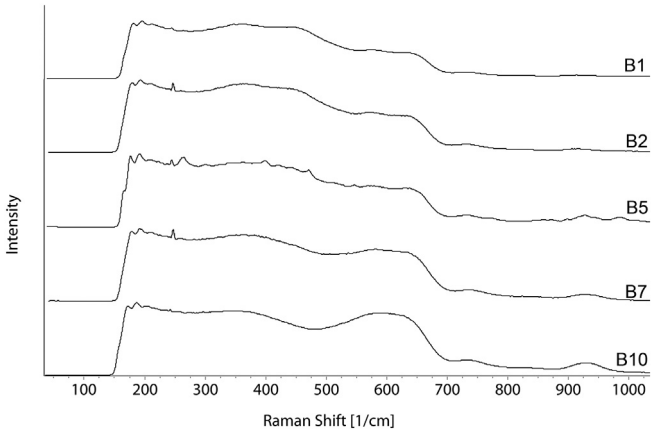

Fig. 7. Raman spectra of the series B (x from 1 to 10 mol%).

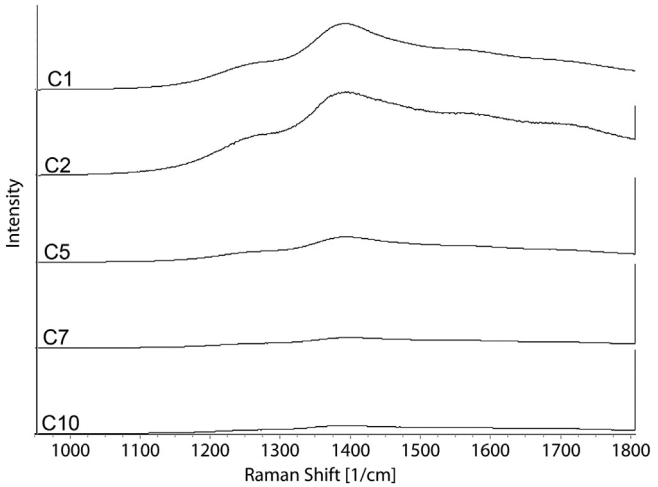

Fig. 8. Raman spectra of the series C (x from 1 to 10 mol%).

that the highest band intensity for this sample is reached above 1200 cm^{-1}. These bands correspond to the stretching vibration of the terminal B—O— bonds of the pyroborates groups [47,48]. The Raman peaks due to the heavy metal oxides such as Bi_2O_3 may be classified into four main groups [49]: low wave number Raman modes (< 100 cm^{-1}), heavy metal ion vibrations (range 70–160 cm^{-1}), bridging anion modes (range 300–600 cm^{-1}) and nonbridging anion modes over 600 cm^{-1}. The bands around 200 cm^{-1} can be associated with the bismuth or barium unit vibrations because generally the heavy metal oxide unit vibrations appear at significantly smaller wave

numbers in comparison with the boron ones [50]. The broad shoulders centered around 300–350 cm^{-1} and 480–580 cm^{-1} can assigned to the Bi—O and Bi—O—Bi vibration in distorted linked [BO_6] polyedra [50]. At 720 cm^{-1} the bending vibration of B—O—B bridges in metaborate chains can contribute to the Raman scattering of metaborate chain group vibrations [51–53]. The almost complete lack of signal in the range 750–1100 suggest that larger superstructural groups are absent in the glass structure or their concentration is very low.

Raman spectra in Fig. 6, related to Dy_2O_3 doped glasses, shows a stronger group of bands in the range comprised to 150 to 700 cm^{-1}. The intensities of these bands are almost constant, when the dopant content is changed even if some difference can be detected. Taking in account samples A5, A7 and A10 a shift to smaller wavenumbers with respect to the other samples, and a variation in shape can be observed for the shoulder around 500 cm^{-1}. This variation can be explained with the arise of $[BO_4]^-$ tetrahedra [47,54–55]. At the same time, for the same samples, in the region above 700 cm^{-1} two small bands increase according to the amount of Dy_2O_3. The shoulder at 720 cm^{-1} can be associated with the symmetric breathing vibrations of six-membered rings (two-ditriborate ring).

Fig. 7 (Er_2O_3 as dopant) is quite similar to the Dy_2O_3 one, the stronger bands are in the range from 150 to 700 cm^{-1} and related to bridging anion vibration modes. In the range from 700 to 1200 cm^{-1} only two bands are detectable for the sample B5. In particular these two bands falls in the range comprised between 740 cm^{-1} and 940 cm^{-1}. These same bands merged in the sample B7 but shifted to lower wavenumber with respect to B5. These bands are typical of larger superstructural groups (910 cm^{-1}). Again for the samples containing above 5% of dopant, B5, B7 and B10 a shift to smaller wavenumbers and a change in shape for the shoulder around 500 cm^{-1} can be observed if compared to the other samples. This variation can be explained with the arise of $[BO_4]^-$ tetrahedra [47,54–55]. Around 620 cm^{-1} two weak bands are visible for the sample B1, and their intensities seems to increase with the increasing of the dopant content. According with this trend in the sample B10 these two bands merged in one stronger band centered at 600 cm^{-1} with relevant higher intensity. This band can be related to Bi-O-Bi vibration in distorted linked [BO_6] polyhedra (580 cm^{-1}). For the other bands, very similar consideration derived for the Dy_2O_3 glasses can be obtained.

In the Raman spectra of the glasses containing Nd_2O_3 (Fig. 8) the stronger bands appear over 1200 cm^{-1} and the intensity of that bands decrease in a linear way with the increasing of the dopant content. For this series of glasses the structure seem to be characterized mostly by the stretching of pyroborate structures, as previously stated for the undoped glass.

3.2. Physical properties: density and molar volume

In Fig. 9 and Fig. 10 respectively the measured densities and calculated molar volumes have been reported. For each property the average values, are related to the amount of dopant for each rare earth with an estimated standard deviation of 1%. It is worth noting that samples showing crystalline phases in structural characterization are reported using white triangular markers because they derived values cannot be directly compared to the other glass samples.

The average density values experimentally obtained falls in the range of 5.8–6.7 g/cm^3 and nonlinear trend as a function of the increasing content of dopant can be observed. About molar volume the average values are in the range 17.5–23.5 cm^3/mol. The higher value of molar volume is detected in the sample without any dopant. On the other hand the molar volume values drop with the Bi_2O_3 content decreasing as consequence of RE increasing. This effect is even more accentuate for the samples in which crystalline phases were detected.

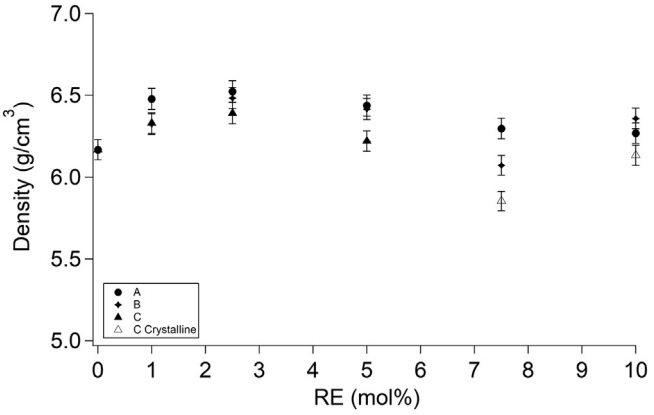

Fig. 9. Density vs RE content (mol%).

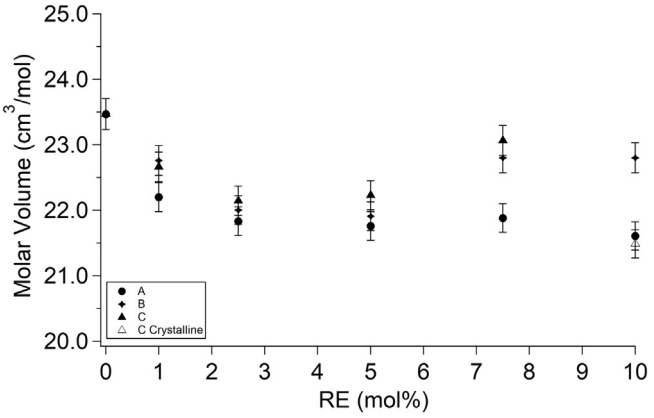

Fig. 10. Molar Volume vs RE content (mol%).

Table 2
Tg Tc and Tm of the investigated glasses (*double peak of crystallization ** double peak of melting, associated uncertain ± 10 °C).

Dopant	Sample	Tg (°C)	Tc (°C)	Tm (°C)
–	U	380	490	660
Dy_2O_3	A1	390	500	690
	A2	410	525	730
	A5	440	550*	800**
	A7	500	610	880
	A10	525	650	950
Er_2O_3	B1	390	500	670
	B2	400	540	680
	B5	430	590	690
	B7	500	630	790
	B10	540	660*	960**
Nd_2O_3	C1	390	460	690
	C2	410	490	820
	C5	450	510	900
	C7	490	530	960
	C10	510	570	980

3.3. Thermal property: DSC

In Table 2 the glass transition temperatures (Tg), the crystallization temperatures (Tc) and the melting temperatures (Tm) have been reported for each glasses investigated. For all the glasses investigated the increasing of the amount of dopant is related with the increase of Tg, Tc and Tm. Furthermore, samples A5 and B10 show two exothermic peaks of crystallization and two endothermic peaks which average values have been reported in Table 2.

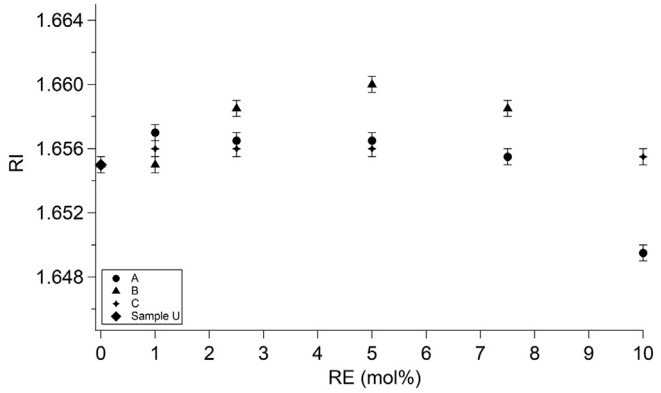

Fig. 11. RI vs RE contents (mol%).

3.4. Optical and scintillating properties: RI, luminescence and scintillation

The values of RI measured as a function of the increasing amount of dopant for each sample are shown in Fig. 11.

It is worth noting that this property has been measured only for the totally glassy sample, because the presence of crystalline phase causes an aberration in the values, which falls out of the range of the instrument used. The instrument sensibility (0.001) has been taken as error on the measured value. It is possible to note that RI generally increases until the content of RE is about 5 mol%. While for the Er_2O_3 series RI does not depend by the dopant concentration, different trend can be noted for the Nd_2O_3 and Dy_2O_3 samples, even if the difference between the samples are very slight. Transmittance has been evaluated in the UV–VIS region for all the samples investigated in this study, as shown in Fig. 12.

As can be seen in this figure no relevant difference can be detected between samples doped with the same dopant, but important difference can be detected considering the different dopants employed. Dy_2O_3 doped glasses shown the best transmittance, because no relevant peak of absorbance can be seen, even if the overall transmittance is below 20%. Only a small peak that can be related with Dy_2O_3 is detected around 450 nm. On the other hand, Er_2O_3 and Nd_2O_3 doped glasses shown the presence of peak of absorbance that can be related with the characteristic peak of the rare earths investigated [20,29]. The difference between the RE can be related with the network modification that produced effects on the energy band gaps of absorption of the glasses.

The luminescent properties are expressed in terms of emission intensity at specific excitation wavelengths, properly choose from literature in consideration of which RE has been employed. According with previous studies and by analyzing the excitation spectra reported in Fig. 13, Fig. 15 and Fig. 17 the wavelengths chosen for our investigation are: 360 nm for Dy_2O_3 glasses [24,56], 514 nm for Nd_2O_3 glasses [21,28,56], 480 nm for Er_2O_3 glasses [20,31]. As concerning series A the small excitation peak (360 nm) reported in Fig. 13 is associated with the state $^6H_{15/2} \rightarrow {}^4I_{11/2}$ [24,56]. In series B the highest peak of the excitation spectra reported in Fig. 15 at 480 nm is related with the state $^4I_{15/2} \rightarrow {}^4F_{7/2}$, whereas the other small peak at about 470 nm to the state $^4I_{15/2} \rightarrow {}^4F_{5/2}, {}^4F_{3/2}$ [20,31]. Finally, in series C (Fig. 17) the peak around 540 nm is associated with the transition from the ground state $^4I_{9/2} \rightarrow {}^4G_{9/2}$ [21,28,56]. Following this method, the luminescence properties of glasses doped with the same rare earth have been measured in the same condition only in the UV–VIS range of the electromagnetic spectrum. The U sample has been measured at three different excitation wavelengths, in order to compare this glass in the same condition for each one of the three groups of glasses. The emission spectra are shown in Fig. 14, Fig. 16 and Fig. 18.

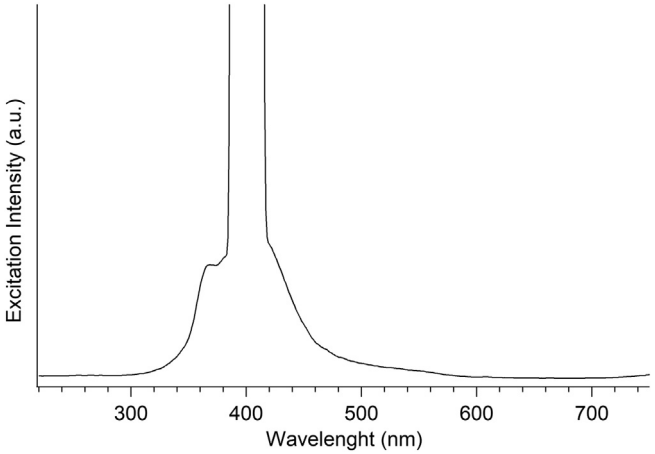

Fig. 13. Excitation spectra for series A (λ = 400 nm).

Considering Fig. 14, Fig. 16 and Fig. 18 it is possible to see that no clear peak can be observed in the UV–VIS region observed but some comparative considerations can be made about the intensity registered near the excitation wavelength. It is possible to see some qualitative difference in the spectra intensity. While for both Dy_2O_3 and Er_2O_3 containing glasses the highest intensity is reached for a content equal to 5 mol% (A5 and B5), for Nd_2O_3 containing glasses the highest intensity is reached for a content equal to 7.5 mol% (C7). This glass shows the highest emission intensity, observing the region of the spectra near the excitation wavelength.

From the analysis of the optical properties, considering in particular the emission intensity results, three glasses (A5, B5 and C7) have been selected and the scintillating properties have been derived. In fig. 19 the comparison between the scintillating light yield of the doped glass samples and the standard blue have been reported and no scintillation peak can been detected.

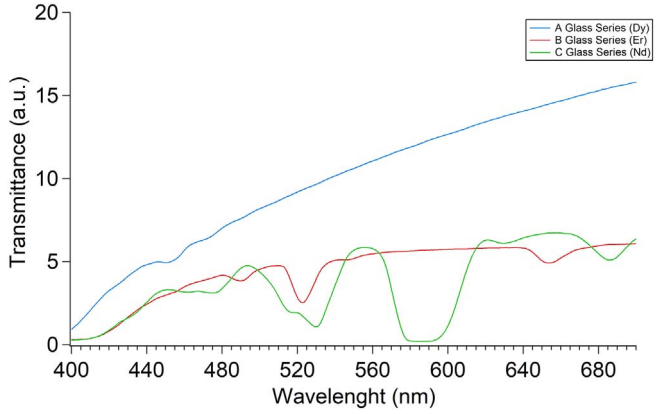

Fig. 12. Transmittance spectra of the investigated glasses.

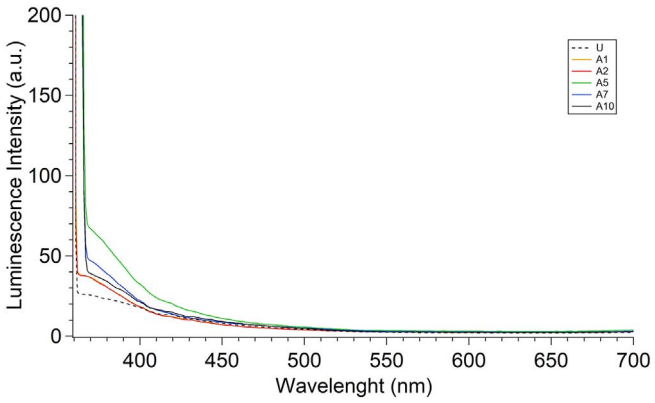

Fig. 14. Luminescence spectra for series A.

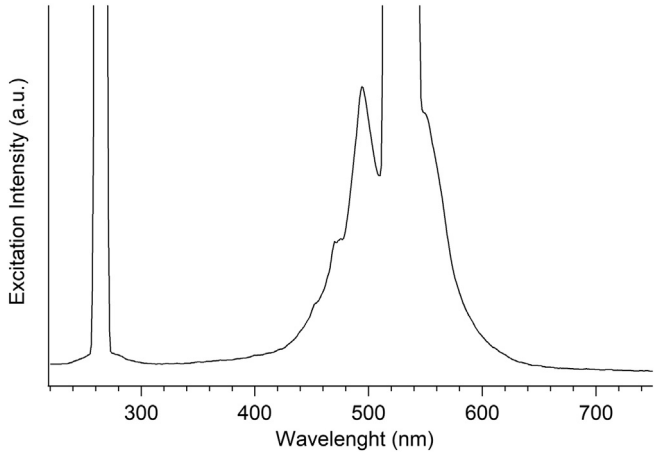

Fig. 15. Excitation spectra for series B (λ = 540 nm).

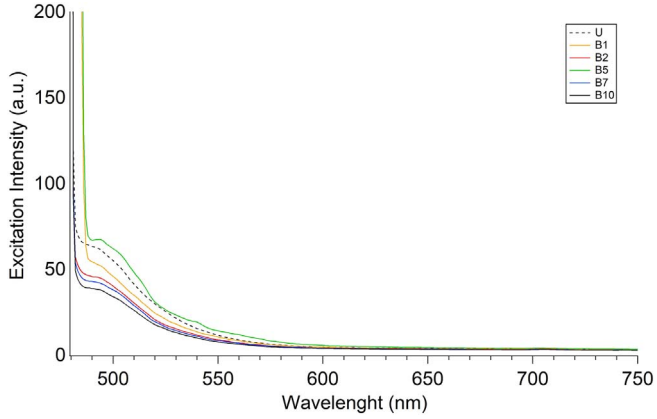

Fig. 16. Luminescence spectra for series B.

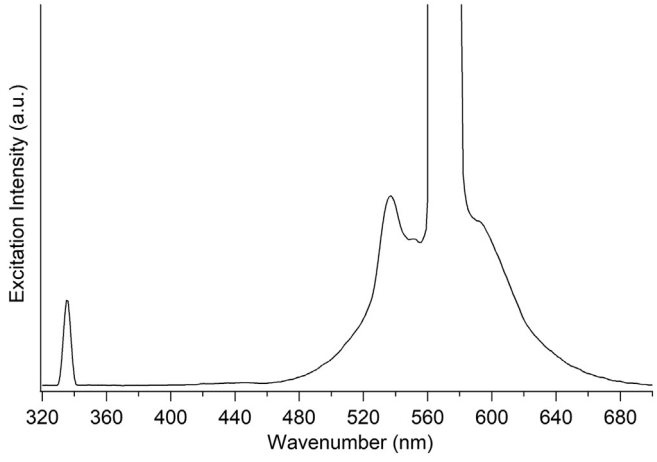

Fig. 17. Excitation spectra for series C (λ = 570 nm).

4. Discussion

Considering the XRD results the glassy broad band at about 28°2θ is typical of borate glass. A strong decreasing of intensity of that band can be observed in almost all the series for the 5 mol% of dopant. It can be supposed that in correspondence of 5 mol% of dopant the glass network moves towards a structural transition resulting into a local and medium environment quite different from the others. Probably the typical boron rings and bridging oxygens connections have been progressively destroyed by the dopant addition [57]. A more detailed consideration

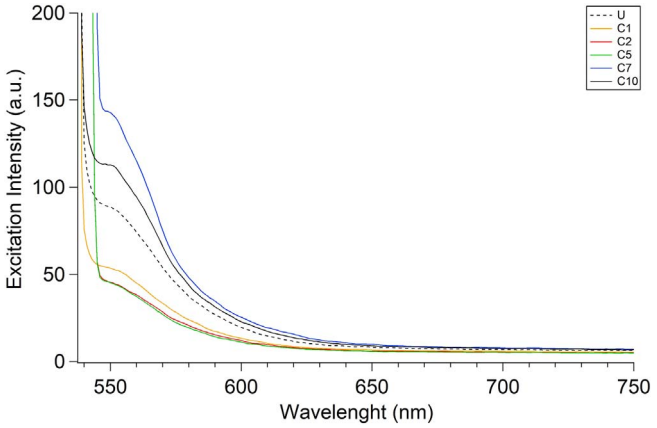

Fig. 18. Luminescence spectra for series C.

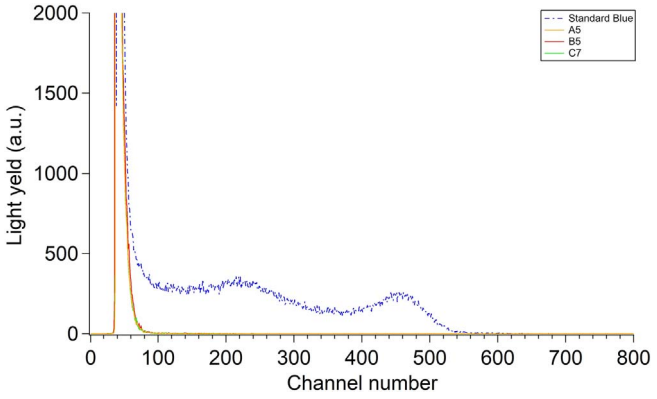

Fig. 19. Light yield spectra of selected doped glasses compared with standard blue. (For interpretation of the references to color in this figure legend, the reader is referred to the web version of this article.)

about the borate structures can be achieved from the Raman spectroscopy analysis. The Krogh-Moe hypothesis is based on the assumption that structural units present in oxide glasses resemble the units present in the corresponding crystalline compounds [58]. This method has been previously taken as the basis for the analysis of Raman results in borate glasses leading good results [58–60]. In this study the increasing content of RE oxides corresponds to a parallel decrease of the Bi_2O_3 amount (Table 1). In the series of spectra characterized by the presence of Dy_2O_3 the main bands can be seen at wavelength below 700 cm^{-1} where mainly the bridging anion modes due to heavy metals are present. This fact supports the network forming character of bismuth [49]. Taking in account the Raman spectra of A5 which present the lower intensity of the glassy band in the XRD spectra, also a complete disappearing of the shoulder near 470 cm^{-1} can be observed. This band can be related to Bi—O—Bi vibration in distorted linked [BO_6] polyhedra [50]. For this reason we can suppose that this specific glass formulation leads to the decrease of the network connections through BO structure. The Raman spectra of the Er_2O_3 series show a strong similarity with the spectra containing Dy_2O_3. The stronger bands of the doped glasses are in the range from 150 to 700 cm^{-1} and related to bridging anion vibration modes. Finally about the samples doped with Nd_2O_3 the most relevant band can be identified in the range from 1200 to 1800 cm^{-1} in strong similarity with the sample U. The intensity of that band seems to decrease in a linear way with the increasing of the dopant content. For this series of glasses the structure seem to be characterized mostly by the stretching of pyroborate structures. No crystallization peak can be detected with this technique, probably due to the fact that the formation of crystalline phases is not so strong as suggested also from the XRD analysis shown in Fig. 4. It can be

concluded that Nd_2O_3 doped glass show a structure more similar to the base glass which is characterized by pyroborate structures. On the opposite, the Er_2O_3 and Dy_2O_3 doped glass seem to have a different structure if compared to the U glass, mainly characterized by bridging anion vibration modes.

The overall results in terms of density (Fig. 9) must be considered positive taking in account the specific requirement for glasses for HEP (> 5 g/cm^3), even if it results quite far from the density reached by lead containing glasses (≈ 8 g/cm^3) [21]. As can be clearly seen from Fig. 9 for each RE oxides considered, density is a nonlinear property in function of the increasing dopant content from 0 to 10 mol%, in fact the highest value of density is reached for a dopant content equal to 2.5%. On the other hand the lowest values of this property are reached for a dopant content of 7.5% for all the considered series. The relationship between structure and density have to consider the weight and the amount of the dopants with respect to the values related to heavy metal oxide that was substituted (Bi_2O_3). For this reason often the molar volume is preferred to achieve further structural information. The molar volume of glasses decreases as a result of more interconnected network characterized by reduced bond length and inter atomic spacing due to the substitution of Bi^{3+} (ionic radio 0.170 nm) with dopants such as Dy^{3+} (0.105 nm), Er^{3+} (0.103 nm) and Nd^{3+} (1.123 nm) [61–62]. This behavior is suggested also by the increasing of the T_g due to rare earth addition. Increasing the amount of dopant over 5 mol% two behaviors can be observed, one with a little but significant increase of molar value is due to the totally glassy nature of the samples, and a second one in which the creation of crystalline phases results in a strong decreasing of molar volume. It is well known that bond distances in crystalline structure are lower than in the glass and this clearly affect the final Vm. As expected from the theoretical relation between density and molar volume, the main trends of these two parameters are inversely proportional and in particular for the series of glasses A the dopant addition is confirmed to increase the density. This result suggest that the changes in structure, detectable also through the molar volume decreasing, have a greater impact on density than the decreasing of the molecular weight of the composition when the bismuth (208,98 u) is substituted with the rare earth (Dy = 162,50 u; Er = 167,26 u Nd = 144.24 u).

At the same time also an increasing of Tg, Tc and Tm can be detected when the dopants are increased into the glass formulation, as confirmation of the reduced molar volume due to dopant increment. Moreover must be considered that the melting temperature of rare earths are in general meaningful higher than the bismuth oxide one, because of this an increasing of dopant effect also the melting temperature of the formulation. Generally, the increase in RI follows the changes observed in the glass structure: the creation of nonbridging oxygen (NBO) due to incorporation of dopant in the glass network strongly affects this properties [33]. In fact, Raman spectra analysis points out the increase of the pyroborate group contribution and therefore the increase of the NBO amount only in the Nd_2O_3 which shows also the higher RI. This result has been also observed in silica glass though experimental and modelling approach [63–64]. It is worth noting that all the refractive index values obtained are consistent with the requirements for HEP glasses, where a small refractive index is needed for the coupling of the glass sensors with other material (i.e. plastic) into the Hadronic calorimeter detector.

The transmittance of light in glass for HEP experiments is extremely important in order to ensure the particle detecting and therefore the signal goodness in order to maximize the efficiency of the detector. For this reason a totally glassy state is favorable and in this perspective Er_2O_3 and Nd_2O_3 doped glasses showed in general the worst transmittance due to the presence of optical absorbance, whereas Dy_2O_3 doped glasses show in general the best results.

From a luminescent spectrum it is possible to evaluate the intensity of an emission phenomenon at a particular wavelength, considering the presence of one or more peaks of emission. In particular, even more high is the peak intensity and stronger is the luminescence. This rule can be applied because in hadronic calorimeter a pulse of light is measured, whereas in other application the area under the peak must be considered. The obtained results point out the absence of any peak of luminescent emission. Although an excitation phenomenon is activate, we must consider the possibility that this particular glass matrix acts as a shield for luminescent emission, absorbing it, in this way all the emission investigated in this study are non-radiative in the UV–VIS region. The scintillation spectra of the investigated glasses as shown in Fig. 19, demonstrate also that an indirect but high energy excitation is not able to produce a detectable emission reaction. In fact, the emission spectra are almost similar to those of luminescence spectra, which implies that energy transfer do not takes place neither under X-ray excitation for all the rare earths employed in this study. But if we compare the luminescent spectra with the Raman results some important indications can be achieved considering the Nd_2O_3 doped glass. It is worth noting that this series of glass shows the best results in terms of luminescent emission due to the intensity of the shoulders near the excitation peaks, despite of the weak transmittance. The same group of glasses is the one related to a structure were the presence of pyroborate groups is more relevant suggesting that the luminescent emission could be enhanced by considering glass structure in which the pyroborates groups are present in high percentages and more relevant that others species.

5. Conclusions

In this study a deep investigation has been made about glasses suitable for hadronic calorimeter. In this field of application high density glasses must satisfy also very specific optical requirements in order to block the particles and to convert its energy into a series of light pulses detectable and measurable. To fit both the scopes heavy metal oxides have been investigated to formulate the glass host, whereas the optical properties have been enhanced with the introduction of rare earths in different amount and type. Very interesting results have been achieved considering the physical properties because high density glasses have been formulated, avoiding the drawbacks of lead glasses, well known as high density materials. In particular avoiding lead is possible to keep the refractive index at quite low level, in the range requested for the coupling with the other materials present into the scintillator. Also the environmental issues due to lead disposal can be avoided. More efforts should be done in order to improve the transmittance and the luminescence intensity. In particular a possible route should be the employment of Dy as dopant, due to its low optical absorbance, in ad hoc glass formulation characterized by a more compact network characterized by homogeneous distribution of heavy metal units, avoiding clustering which results into the decrease/ disappearing of the luminescence signal in the UV–VIS region. In this perspective, and based on the obtained statements, several test using different glass and different heavy metal oxide in the glass formulation will be planned to promote the formation of pyroborate units and enhance the optical transmittance.

Acknowledgements

This work have been partially founded by Italian National Institute for Nuclear Physics – Naples section. The scientific program “T1015 Collaboration” at Fermilab and the “TWICE project” are greatly acknowledged.

References

[1] T.A. Edison, Nature 470 (1896).
[2] M. Levy, Fortschr. Geb. Rontgenstr. 1 (1897) 75.
[3] E. Rutherford, J. Chadwich, C.D. Ellis, Radiations from Radioactive Substances, Cambridge University Press, Cambridge, 1930.

[4] L3 Collaboration, Adeva B, et al., The construction of the L3 experiment, Nucl. Instrum. Methods Phys. Res. A289 (1990) 35–102.
[5] Y. Kubota, et al., The CleoII Detector, CLNS 91/1122, (1991).
[6] C. Amsler, Proton-antiproton annihilation and meson spectroscopy with the crystal barrel, Rev. Mod. Phys. 70 (1998) 1293.
[7] R. Re, The KTeV Pure CsI Calorimeter, Proc. Fifth International Conference on Calorimetry in High-Energy Physics, World Scientific, New Jersey, 1994, pp. 110–114.
[8] The Belle Collaboration, Technical Design Report, KEK Report 95-1, (1995).
[9] The BaBar Collaboration, BaBar Technical Design Report, SLAC-R-95-457, (1995).
[10] R. Novotny, R. Riess, R. Hingmann, Detection of hard photons with BaF2 scintillators, Nucl. Instrum. Methods Phys. Res. A262 (1987) 340–346.
[11] GEM Letter of Intent, SSCL SR-1184, November (1991).
[12] CMS Technical Proposal, CERN/LHCC 94-38, December (1994).
[13] L3P Letter of Intent, CERN/LHCC 92-5, (1992).
[14] ALICE Collaboration Technical Proposal, CERN/LHCC/95-71, (1995).
[15] P. Lecoq, A. Annenkov, A. Gektin, M. Korzhik, C. Pedrini, Inorganic Scintillators for Detectors Systems: Physical Principles and Crystal Engineering, Springer, the Netherlands, 2006.
[16] M.J. Weber, Inorganic scintillators: today and tomorrow, J. Lumin. 100 (2002) 35–45.
[17] J. Fu, M. Kobayashi, J.M. Parker, Terbium-activated heavy scintillating glasses, J. Lumin. 128 (2008) 99–104.
[18] Y. Zhang, N. Ding, T. Zheng, S. Jiang, B. Han, Effects of Ce^{3+} sensitizer on the luminescent properties of Tb^{3+}-activated silicate oxyfluoride scintillating glass under UV and X-ray excitation, J. Non-Cryst. Solids 441 (2016) 74–78.
[19] A.J. Kenyon, Recent developments in rare-earth doped materials for optoelectronics, Prog. Quantum Electron. 26 (2002).
[20] I.I. Oprea, H. Hesse, K. Betzler, Luminescence of erbium-doped bismuth-borate glasses, Opt. Mater. 28 (2006) 1136–1142.
[21] S. Mohan, K.S. Thind, D. Singh, L. Gerward, Optical properties of alkali and alkaline-earth lead borate glasses doped with Nd^{3+} ions, Phys. Chem. 34 (2008) 265–273.
[22] G.C. Righini, M. Ferrari, Photoluminescence of rare-earth-doped glasses, Riv. Nuovo Cimento Soc. Ital. Fis. 28 (2005) 1–53.
[23] S. Insitipong, J. Kaewkhao, T. Ratana, P. Limsuwan, Optical and structural investigation of bismuth borate glasses doped with Dy^{3+}, Procedia Eng. 8 (2011) 195–199.
[24] J. Pisarska, Luminescence behavior of Dy^{3+} ions in lead borate glasses, Opt. Mater. 31 (2009) 1784–1786.
[25] K. Nanda, N. Berwal, R.S. Kundu, R. Punia, N. Kishore, Effect of doping of Nd^{3+} ions in BaO–TeO_2–B_2O_3 glasses: a vibrational and optical study, J. Mol. Struct. 1088 (2015) 147–154.
[26] S. Tanabe, Optical transitions of rare earth ions for amplifiers: how the local structure works in glass, J. Non-Cryst. Solids 259 (1999) 1–9.
[27] U. Rambabu, N.R. Munirathnam, T.L. Prakash, S. Buddhudu, Emission spectra of $LnPO_4$:RE^{3+} (Ln = La, Gd; RE = Eu, Tb and Ce) powder phosphors, Mater. Chem. Phys. 78 (2003) 160–169.
[28] J. Pisarska, W.A. Pisarski, G. Dominiak-Dzik, W. Ryba-Romanowski, Spectroscopic investigations of Nd^{3+} ions in B_2O_3-PbO-Al_2O_3-WO_3 glasses, J. Mol. Struct. 792 (2006) 201–206.
[29] M. Farouk, A. Samir, F. Metawe, M. Elokr, Optical absorption and structural studies of bismuth borate glasses containing Er^{3+} ions, J. Non-Cryst. Solids 371 (2013) 14–21.
[30] W.A. Pisarski, T. Goryczka, B. Wodecka-Dus, M. Plonska, J. Pisarska, Structure and properties of rare earth-doped lead borate glasses, Mater. Sci. Eng. B 122 (2005) 94–99.
[31] J. Janek, Luminescence investigations of rare earth doped lead-free borate glasses modified by MO ($M_{1/4}$ Ca, Sr, Ba), Mat, Chem. Phys. 180 (2016) 237–243.
[32] Y.D. Yiannopoulos, G.D. Chryssikos, E.I. Kamitsos, Structure and properties of alkaline earth borate glasses, Phys. Chem. Glasses 42 (2001) 164–172.
[33] S. Shiv Prakash, K. Basudeb, Bismuth oxide and bismuth oxide doped glasses for optical and photonic applications, Bismuth: Characteristics, Production and Applications, Materials Science and Technologies, Nova, Hauppauge, New York, 2012(ISBN 978-1-61470-640-3).
[34] H.T. Sun, J. Zhou, J. Qiu, Recent advances in bismuth activated photonic materials, Prog. Mater. Sci. 64 (2014) 1–72.
[35] S.M. Lakiza, J.S. Tyschenko, L.M. Lopato, Phase Diagram of the Al_2O_3 – HfO_2 – Y_2O_3 system, 31 (2011), pp. 1285–1291.
[36] E.S. Yousef, A. El-Adawy, N. El-KheshKhany, Effect of rare earth (Pr_2O_3, Nd_2O_3, Sm_2O_3, Eu_2O_3, Gd_2O_3 and Er_2O_3) on the acoustic properties of glass belonging to bismuth-borate system, Solid State Commun. 139 (2006) 108–113.
[37] C. Mugoni, C. Gatto, A. Pla-Dalmau, C. Siligardi, Structure and luminescence properties of Dy_2O_3 doped bismuth- borate glasses, J. Non-Cryst. Solids 471 (2017) 295–300.
[38] O. Sanz, E. Haro-Poniatowski, J. Gonzalo, J.M. Fernandez Navarro, Influence of the melting conditions of heavy metal oxide glasses containing bismuth oxide on their optical absorption, J. Non-Cryst. Solids 352 (2006) 761–768.
[39] M. Peng, D. Chen, J. Qiu, X. Jiang, C. Zhu, Bismuth-doped zinc aluminosilicate glasses and glass-ceramics with ultra-broadband infrared luminescence, Opt. Mater. 29 (2007) 556–561.
[40] Y. Fujimoto, M. Nakatsuka, Optical amplification in bismuth-doped silica glass, Appl. Phys. Lett. 82 (2003) 3325.
[41] Y. Arai, T. Suzuki, Y. Ohishi, S. Morimoto, S. Khonthon, Ultrabroadband near-infrared emission from a colorless bismuth-doped glass, Appl. Phys. Lett. 90 (2007) 2611.
[42] H.P. Xia, X.J. Wang, Near infrared broadband emission from Bi^{5+}-doped Al_2O_3–GeO_2–X (X = Na_2O, BaO, Y_2O_3) glasses, Appl. Phys. Lett. 89 (2006) 51.
[43] M. Peng, J. Qiu, D. Chen, X. Meng, I. Yang, X. Jiang, C. Zhu, Bismuth and aluminum-codoped germanium oxide glasses for super-broadband optical amplification, Opt. Lett. 29 (2004) 1998–2000.
[44] S.P. Singh, R.P.S. Chakradhar, J.L. Rao, B. Karmakar, F.T.I.R. EPR, Optical absorption and photoluminescence studies of Fe_2O_3 and CeO_2 doped ZnO–Bi_2O_3–B_2O_3 glasses, J. Alloys Compd. 493 (2010) 256–262.
[45] S.P. Singh, R.P.S. Chakradhar, J.L. Rao, B. Karmakar, EPR, optical absorption and photoluminescence properties of MnO_2 doped $23B_2O_3$–5ZnO–$72Bi_2O_3$ glasses, Physica B 405 (2010) 2157–2161.
[46] A.D. Bross, A. Pla-Dalmau, B. Baumbaugh, J. Godfrey, J. Jaques, J. Marchant, Development and characterization of new scintillation materials for fiber tracking and calorimetry, Nucl. Instrum. Methods Phys. Res., Sect. A 4 (1991) 35–46.
[47] E.I. Kamitsos, M.A. Karakassides, G.D. Chryssikos, Phys. Chem. Glasses 30 (1989) 229–234.
[48] B.N. Meera, J. Ramakrishna, Raman spectral studies of borate glasses, J. Non-Cryst. Solids 159 (1993) 1.
[49] L. Baia, R. Stafan, W. Kiefer, J. Popp, S. Simon, Structural investigation of copper doped B_2O_3-Bi_2O_3 glasses with high bismuth oxide content, J. Non-Cryst. Solids 303 (2002) 379–386.
[50] A.A. Kharlamov, R.M. Almeida, J. Heo, J. Non-Cryst. Solids 202 (1996) 233.
[51] A.C. Wright, Phys. Chem. Glasses Eur. J. Glass Sci. Technol. B 51 (2010) 1–39.
[52] G.D. Chryssikos, E.I. Kamistos, A.P. Patsis, M.S. Bitsis, M.A. Karakassies, J. Non-Cryst. Solids 126 (1990) 42–51.
[53] A. Rulmont, M. Almou, Spectrochim. Acta 45A (1989) 603–610.
[54] Y.D. Yiannopoulos, G.D. Chryssikos, E.I. Kamitsos, Phys. Chem. Glasses 42 (2001) 164–172.
[55] B.P. Dwivedi, M.H. Rahman, Y. Kumar, B.N. Khanna, J. Phys. Chem. Solids 55 (1993) 621–628.
[56] J. Pisarska, W.A. Pisarski, W. Ryba-Romanowski, Laser spectroscopy of Nd^{3+} and Dy^{3+} ions in lead borate glasses, Opt. Laser Technol. 42 (2010) 805–809.
[57] B.E. Warre, X-ray diffraction study of the structure of glass, Chem. Rev. 26 (2) (1940) 237–255.
[58] J. Krogh-Moe, The structure of vitreous and liquid boron oxide, J. Non-Cryst. Solids 1 (1969) 269–284.
[59] T.G. Kujumzelis, Raman effect and glass structure, Z. Phys. 100 (1936) 221–236, http://dx.doi.org/10.1007/BF01418605.
[60] W. Konijnendijk, J.M. Stevels, The structure of borate glasses studied by Raman scattering, J. Non-Cryst. Solids 18 (1975) 307.
[61] I.I. Oprea, H. Hesse, K. Betzler, Optical properties of bismuth borate glasses, Opt. Mater. 26 (2004) 235–237.
[62] R.D. Shannon, Revised effective ionic radii and systematic studies of interatomic distances in halides and chaleogenides, Acta Cryst A32 (1976) 751.
[63] A. Bonamartini Corradi, V. Cannillo, M. Montorsi, C. Siligardi, A.N. Cormack, Structural characterization of neodymium containing glasses by molecular dynamics simulation, J. Non-Cryst. Solids 351 (2005) 1185–1191.
[64] A. Bonamartini Corradi, V. Cannillo, M. Montorsi, C. Siligardi, Influence of Al_2O_3 addition on thermal and structural properties of erbium doped glasses, J. Mater. Sci. 41 (2006) 2811–2819.